The 8th European Congress on Computational Methods in Applied Sciences and Engineering
ECCOMAS Congress 2022
5-–9 June 2022, Oslo, Norway

A GRADIENT-EXTENDED ANISOTROPIC DAMAGE-PLASTICITY MODEL IN THE LOGARITHMIC STRAIN SPACE

HAGEN HOLTHUSEN*, TIM BREPOLS*, JAAN-WILLEM SIMON* AND STEFANIE REESE*

* Institute of Applied Mechanics (IFAM)
RWTH Aachen University
Mies-van-der-Rohe-Str. 1, D-52074 Aachen, Germany
e-mail: holthusen@ifam.rwth-aachen.de, web page: https://www.ifam.rwth-aachen.de

Key words: Anisotropic damage, Damage tensor, Gradient damage-plasticity, Micromorphic approach, Finite strains, Mesh regularization

Abstract. Within this contribution, we discuss additional theoretical as well as numerical aspects of the material model developed in [1, 2], where a 'two-surface' damage-plasticity model is proposed accounting for induced damage anisotropy by means of a second order damage tensor. The constitutive framework is stated in terms of logarithmic strain measures, while the total strain is additively decomposed into elastic and plastic parts. Moreover, a novel gradient-extension based on the damage tensor's invariants is presented using the micromorphic approach introduced in [3]. Finally, going beyond the numerical examples presented in [1, 2], we study the model's ability to cure mesh-dependency in a three-dimensional setup.

1 INTRODUCTION

The defects observed on the microstructure can be classified into microvoids and microcracks, the former degrading the material more or less directionally independent. The latter, on the other hand, induce a strong anisotropy even in initially isotropic materials. Continuum mechanical models that take this anisotropy into account are essential for estimating the stiffness, and thus, the load-bearing capacity of structures that are damaged. In this context, non-proportional load paths, such as those occurring in forming processes, are also known to trigger this kind of induced anisotropy.

Within this contribution, in line with Continuum Damage Mechanics (CDM), we account for damage anisotropy by means of a second order damage tensor (see [4]) in a phenomenological and smeared sense. The CDM modeling approach is used for a wide range of materials and damage behaviors, ranging from initially isotropic materials (e.g. [5]) to initially anisotropic materials with different constituents (e.g. [6]), and further, is employed in the context of scale transitions (e.g. [7]). In this regard, [8] recently formulated a finite strain framework that interprets the second order damage tensor in terms of structural tensors. This approach is also followed in [1, 2], but in the logarithmic strain space, where additionally a novel gradient-extension is introduced. The latter extension is necessary to overcome mesh-dependency, a well-known problem

of so-called local damage models, to which the class of CDM models belongs. In view of the many possibilities known in the literature for introducing a gradient-extension, the latter authors decided to use the micromorphic approach [3, 9], which provides a rather flexible and general framework for introducing additional length scales into the material formulation.
In this contribution, we first consider various aspects of the model developed in [1], discussing here in further detail the invariance to superimposed rotations of the intermediate configuration. In addition, the assumption of an additive decomposition of the total strain and the choice of local variables for the gradient extension are briefly discussed (Sec. 2). In Sec. 3, the transformation from logarithmic strain space to the Lagrangian one is presented, where a numerically more efficient calculation method is addressed. Finally, the model is investigated in a three-dimensional context using a tensile specimen (Sec. 4).

2 CONSTITUTIVE FRAMEWORK

Additive decomposition. In finite elasto-plasticity modeling, the multiplicative decomposition $\boldsymbol{F} = \boldsymbol{F}_e\boldsymbol{F}_p$ into elastic and plastic parts is well established, which introduces an intermediate configuration in addition to the reference and current configuration. Further, both parts possess their polar decompositions into a rotational and stretch tensor, i.e. $\boldsymbol{F}_e = \boldsymbol{R}_e\boldsymbol{U}_e$ and $\boldsymbol{F}_p = \boldsymbol{R}_p\boldsymbol{U}_p$ with $\boldsymbol{R}_{e/p} \in \mathrm{SO}(3)$. Since both stretch tensors are defined with respect to different configurations, we make further use of the polar decomposition $\boldsymbol{F}_p = \boldsymbol{V}_p\boldsymbol{R}_p$. These stretch tensors are suitable to define the following logarithmic strain measures

$$\boldsymbol{\varepsilon} \coloneqq \ln(\boldsymbol{U}), \quad \boldsymbol{\varepsilon}_p \coloneqq \ln(\boldsymbol{U}_p), \quad \boldsymbol{\eta}_e \coloneqq \ln(\boldsymbol{U}_e), \quad \boldsymbol{\eta}_p \coloneqq \ln(\boldsymbol{V}_p) = \boldsymbol{R}_p\, \boldsymbol{\varepsilon}_p\, \boldsymbol{R}_p^T \tag{1}$$

where the polar decomposition of the deformation gradient $\boldsymbol{F} = \boldsymbol{R}\boldsymbol{U}$ with $\boldsymbol{R} \in \mathrm{SO}(3)$ is utilized. Considering both the property of the logarithm $\ln(\boldsymbol{A}) = 1/2 \ln\left(\boldsymbol{A}^2\right)$ for any positive definite tensor $\boldsymbol{A}$ and $\boldsymbol{U}_e^2 = \boldsymbol{F}_p^{-T}\boldsymbol{U}^2\boldsymbol{F}_p^{-1}$, one may rewrite the elastic logarithmic strain as

$$\boldsymbol{\eta}_e = \frac{1}{2}\ln\left(\boldsymbol{U}_e^2\right) = \boldsymbol{R}_p\, \frac{1}{2}\ln\left(\boldsymbol{U}_p^{-1}\boldsymbol{U}^2\boldsymbol{U}_p^{-1}\right) \boldsymbol{R}_p^T =: \boldsymbol{R}_p\, \boldsymbol{\varepsilon}_e\, \boldsymbol{R}_p^T \tag{2}$$

where $\boldsymbol{\varepsilon}_e$ is the elastic strain measure with respect to the reference configuration, which is pushed to the intermediate one by $\boldsymbol{R}_p$. Having further the properties $\ln\left(\boldsymbol{A}^{-1}\right) = -\ln(\boldsymbol{A})$ as well as $\ln(\boldsymbol{A}\boldsymbol{B}) = \ln(\boldsymbol{A}) + \ln(\boldsymbol{B})$ if and only if $\boldsymbol{A}$ and $\boldsymbol{B}$ commute in mind, the additive decomposition of the strain is motivated

$$\bar{\boldsymbol{\eta}}_e \coloneqq \boldsymbol{R}_p\,(\boldsymbol{\varepsilon} - \boldsymbol{\varepsilon}_p)\,\boldsymbol{R}_p^T =: \boldsymbol{R}_p\, \bar{\boldsymbol{\varepsilon}}_e\, \boldsymbol{R}_p^T. \tag{3}$$

Obviously, $\boldsymbol{\eta}_e$ and $\bar{\boldsymbol{\eta}}_e$, and thus also $\boldsymbol{\varepsilon}_e$ and $\bar{\boldsymbol{\varepsilon}}_e$, are only equal in case of coaxial loading. However, assuming small elastic strains, the additive decomposition is suitable to capture the elastic strains within the material (cf. [10]). Noteworthy, [11] investigated the additive split in the context of excessive strains for coaxial and non-coaxial loading coupled to damage and provided interesting results on the structural performance.

Mapping of damage tensor. In line with [8], we assume a symmetric and semi-positive definite referential damage tensor $\boldsymbol{D}_r$, which is pushed to the intermediate configuration in analogy to $\boldsymbol{\varepsilon}_e$, $\bar{\boldsymbol{\varepsilon}}_e$ and $\boldsymbol{\varepsilon}_p$

$$\boldsymbol{D} = \boldsymbol{R}_p\, \boldsymbol{D}_r\, \boldsymbol{R}_p^T. \tag{4}$$

Hence, the eigenvalues of both tensors remain the same, while their eigenvectors are transformed by $\boldsymbol{R}_p$. Further, the mapping (4) prevents undesired inelastic scaling effects. Besides these properties, a virgin material is characterized by $\boldsymbol{D}_r = \boldsymbol{D} = \boldsymbol{0}$, while a 'fully broken' state corresponds to $\boldsymbol{D}_r = \boldsymbol{D} = \boldsymbol{I}$.

Rotational non-uniqueness. The multiplicative decomposition of the deformation gradient suffers from an inherent problem of rotational non-uniqueness. Hence, a decomposition including superimposed rotations of the intermediate configuration in the sense of

$$\boldsymbol{F} = \boldsymbol{F}_e \boldsymbol{F}_p = \boldsymbol{F}_e \boldsymbol{Q}^T \boldsymbol{Q} \boldsymbol{F}_p =: \boldsymbol{F}_e^* \boldsymbol{F}_p^*, \quad \boldsymbol{Q} \in \mathrm{SO}(3) \tag{5}$$

can be equivalently stated. Considering the polar decomposition of $\boldsymbol{F}_p^* = \boldsymbol{Q}\boldsymbol{F}_p = \boldsymbol{Q}\boldsymbol{R}_p\boldsymbol{U}_p = \boldsymbol{R}_p^*\boldsymbol{U}_p$ where $\boldsymbol{R}_p^* \in \mathrm{SO}(3)$, one recognizes that this non-uniqueness only affects $\boldsymbol{R}_p$, while $\boldsymbol{U}_p$ is uniquely defined. In further consequence, for the mapping chosen in Equation (4), one must ensure that the Helmholtz free energy ψ is independent of the rotational non-uniqueness, in order to obtain a physically reasonable material formulation, i.e.

$$\psi\left(\bar{\boldsymbol{\eta}}_e, \boldsymbol{\eta}_p, \boldsymbol{D}\right) = \psi\left(\bar{\boldsymbol{\eta}}_e^*, \boldsymbol{\eta}_p^*, \boldsymbol{D}^*\right) \tag{6}$$

with $\bar{\boldsymbol{\eta}}_e^* = \boldsymbol{R}_p^* \left(\boldsymbol{\varepsilon} - \boldsymbol{\varepsilon}_p\right) \boldsymbol{R}_p^{*^T}$, $\boldsymbol{\eta}_p^* = \boldsymbol{R}_p^* \boldsymbol{\varepsilon}_p \boldsymbol{R}_p^{*^T}$, and $\boldsymbol{D}^* = \boldsymbol{R}_p^* \boldsymbol{D}_r \boldsymbol{R}_p^{*^T}$. Therefore, we assume the Helmholtz free energy to be a *scalar-valued isotropic function* of its arguments. Since the following relations hold true

$$\begin{aligned} \mathrm{tr}\left((\bar{\boldsymbol{\eta}}_e^*)^a\right) = \mathrm{tr}\left((\bar{\boldsymbol{\eta}}_e)^a\right), \ \mathrm{tr}\left(\left(\boldsymbol{\eta}_p^*\right)^a\right) = \mathrm{tr}\left((\boldsymbol{\eta}_p)^a\right), \ \mathrm{tr}\left((\boldsymbol{D}^*)^a\right) = \mathrm{tr}\left((\boldsymbol{D})^a\right), \quad a \in \{1,2,3\} \\ \mathrm{tr}\left((\bar{\boldsymbol{\eta}}_e)^b \left(\boldsymbol{\eta}_p\right)^c \left(\boldsymbol{D}\right)^d\right) = \mathrm{tr}\left((\bar{\boldsymbol{\eta}}_e^*)^b \left(\boldsymbol{\eta}_p^*\right)^c \left(\boldsymbol{D}^*\right)^d\right), \quad b,c,d \in \{0,1,2\} \end{aligned} \tag{7}$$

the presented framework using the mapping (4) indeed is invariant with respect to superimposed rotations of the intermediate configuration.

Choice of local variables for gradient-extension The micromorphic approach introduced in [3, 9] introduces a set of 'non-local' variables $\bar{\mathbf{d}}$ on a global level. These variables are strongly coupled to the same number of inherent variables of the material formulation, which will be referred as 'local' variables $\mathbf{d}$. Noteworthy, the latter mentioned should not be understood as additional constitutive variables rather than the constitutive variables themselves or functions of those. Here, three 'local' variables are introduced, which are chosen as the invariants of the damage tensor

$$\mathbf{d} = \left(\mathrm{tr}\left(\boldsymbol{D}\right), \mathrm{tr}\left(\boldsymbol{D}^2\right), \mathrm{tr}\left(\boldsymbol{D}^3\right)\right). \tag{8}$$

Besides the invariant-based gradient-extension, several other possibilities are known in the literature, for instance, enhancing the damage hardening variable (see [12]) or the components of the damage tensor (see e.g. [13]). Although the invariant-based approach is quite general, the question arises whether it is possible to reduce the number of variables. Having in mind that the volumetric part of the damage tensor represents isotropic damage, while the remaining deviatoric part is responsible for the anisotropic nature, one might use the following set

$$\mathbf{d} = \left(\frac{\mathrm{tr}\left(\boldsymbol{D}\right)}{3}, \mathrm{tr}\left(\mathrm{dev}\left(\boldsymbol{D}\right)^2\right)\right) \tag{9}$$

which is a novel approach in gradient-extended anisotropic damage. A further benefit of this latter choice is that it reduces to the gradient-extension proposed by [14] in case of isotropic damage. However, investigating this kind of approach in further detail is out of the scope of this contribution.

2.1 Helmholtz free energy

In the following, the Helmholtz free energy is assumed to be additively decomposable

$$\psi = \psi_e\left(\bar{\boldsymbol{\eta}}_e, \boldsymbol{D}\right) + \psi_p\left(\boldsymbol{\eta}_p, \boldsymbol{D}, \kappa_p\right) + \psi_d\left(\boldsymbol{D}, \kappa_d\right) + \psi_{\bar{d}}\left(\mathbf{d}, \bar{\mathbf{d}}, \mathrm{Grad}\left(\bar{\mathbf{d}}\right)\right) \tag{10}$$

where ψ_e represents the elastically stored energy, ψ_p takes kinematic and isotropic plastic hardening into account, damage hardening is given by ψ_d, and $\psi_{\bar{d}}$ is a 'coupling' or 'non-local' energy term ensuring both a strong coupling between $\mathbf{d}$ and $\bar{\mathbf{d}}$ as well as introduces an internal length scale into the material formulation. Moreover, ψ_d prevents the eigenvalues of $\boldsymbol{D}$ and $\boldsymbol{D}_r$ to exceed the value one and is in line with [12]. Additionally, κ_p and κ_d represent scalar hardening variables for plasticity and damage, respectively.

2.2 Micromorphically extended Clausius-Duhem inequality

Evaluating the micromorphically extended Clasuius-Duhem inequality in the logarithmic strain space

$$-\dot{\psi} + \boldsymbol{T} : \dot{\boldsymbol{\varepsilon}} + \underbrace{\boldsymbol{\xi}_{0_i} \cdot \dot{\bar{\mathbf{d}}} + \boldsymbol{\Xi}_{0_i} : \mathrm{Grad}\left(\dot{\bar{\mathbf{d}}}\right)}_{\text{micromorphic extension}} \geq 0 \tag{11}$$

by inserting the assumed Helmholtz free energy in Equation (10), the following reduced dissipation inequality is obtained

$$\left(\boldsymbol{T} - \boldsymbol{X}\right) : \dot{\boldsymbol{\varepsilon}}_p + R_p\, \dot{\kappa}_p + \boldsymbol{Y} : \dot{\boldsymbol{D}}_r + R_d\, \dot{\kappa}_d \geq 0 \tag{12}$$

under consideration of the state laws

$$\boldsymbol{T} = \boldsymbol{R}_p^T \frac{\partial \psi}{\partial \bar{\boldsymbol{\eta}}_e} \boldsymbol{R}_p, \quad \boldsymbol{\xi}_{0_i} = \frac{\partial \psi}{\partial \bar{\mathbf{d}}}, \quad \boldsymbol{\Xi}_{0_i} = \frac{\partial \psi}{\partial \mathrm{Grad}\left(\bar{\mathbf{d}}\right)}. \tag{13}$$

In Equation (11), $\boldsymbol{T}$ is the 'material' stress work-conjugated to the logarithmic strain rate, while both $\boldsymbol{\xi}_{0_i}$ and $\boldsymbol{\Xi}_{0_i}$ are so-called 'generalized' stresses. The thermodynamically consistent driving forces occurring in Equation (12) can be clearly distinguished into plastic and damage parts. First, we introduce the following plastic driving forces

$$\boldsymbol{X} \coloneqq \boldsymbol{R}_p^T \frac{\partial \psi}{\partial \boldsymbol{\eta}_p} \boldsymbol{R}_p, \quad R_p \coloneqq -\frac{\partial \psi}{\partial \kappa_p} \tag{14}$$

with $\boldsymbol{X}$ being the plastic backstress tensor and R_p the plastic isotropic hardening force. Furthermore, the damage driving forces are obtained as

$$\boldsymbol{Y} \coloneqq -\boldsymbol{R}_p^T \frac{\partial \psi}{\partial \boldsymbol{D}} \boldsymbol{R}_p, \quad R_d \coloneqq -\frac{\partial \psi}{\partial \kappa_d} \tag{15}$$

where $\boldsymbol{Y}$ is the damage driving force and R_d being a damage hardening force. It should be noted that $\boldsymbol{Y}$ is composed out of four individual contribution, which result from the elastic, plastic, damage hardening, and 'non-local' energy terms. For the latter, it is important to note that $\mathbf{d}$ is a function that depends solely on $\boldsymbol{D}$. Hence, the arguments of the 'non-local' energy in Equation (10) can be written as $\psi_{\bar{d}} = \bar{\psi}_{\bar{d}}\left(\boldsymbol{D}, \bar{\mathbf{d}}, \mathrm{Grad}\left(\bar{\mathbf{d}}\right)\right)$. Moreover, it is worth noted that the plastic rotation tensor $\boldsymbol{R}_p$ remains undetermined in the present framework, which is considered an advantage. In order to guarantee that the dissipation inequality is fulfilled for arbitrary processes, meaningful evolution equations are chosen in the following, whereby a 'two-surface' approach is followed. These particular choices, however, do not restrict the generality of the model in any way.

Plastic regime. For the plastic regime, a von Mises-type yield criterion is chosen with respect to the so-called effective continuum

$$\Phi_p \coloneqq \sqrt{3\,\tilde{J}_2} - (\sigma_{y0} - \tilde{R}_p) \leq 0, \quad \tilde{J}_2 \coloneqq \left(\frac{1}{2}\mathrm{tr}\left(\mathrm{dev}\left(\boldsymbol{T} - \boldsymbol{X}\right)^2\right)\right)\Big|_{\boldsymbol{D}=\boldsymbol{0}}, \quad \tilde{R}_p = R_p\Big|_{\boldsymbol{D}=\boldsymbol{0}} \tag{16}$$

with σ_{y0} denoting the plastic onset. For the evolution equations, the principle of maximum dissipation is followed, i.e.

$$\dot{\boldsymbol{\varepsilon}}_p = \dot{\gamma}_p \frac{\partial \Phi_p}{\partial \boldsymbol{T}} = \dot{\gamma}_p\, \mathbb{M}^{-1} : \frac{\partial \Phi_p}{\partial \tilde{\boldsymbol{T}}}, \quad \dot{\kappa}_p = \dot{\gamma}_p \frac{\partial \Phi_p}{\partial R_p} = \frac{\dot{\gamma}_p}{f_d}, \quad \mathbb{M} \coloneqq \frac{\partial \boldsymbol{T}}{\partial \tilde{\boldsymbol{T}}} \tag{17}$$

where $\mathbb{M}$ is a fourth order damage mapping tensor, which transforms the constitutively dependent variables from the effective to the 'damaged' space. Further, $\dot{\gamma}_p$ is the plastic multiplier, while f_d denotes the scalar degradation function and will be introduced in Section 2.3. Karush-Kuhn-Tucker (KKT) conditions close the set of plastic constitutive equations.

Damage regime. In analogy to the plastic regime, the onset of damage is characterized by

$$\Phi_d \coloneqq \sqrt{3\,\boldsymbol{Y}_+ : \mathbb{A}_d : \boldsymbol{Y}_+} - (Y_0 - R_d) \leq 0 \tag{18}$$

with the damage threshold Y_0 and

$$\boldsymbol{Y}_+ = \sum_{i=1}^{3} \langle Y_i \rangle\, \boldsymbol{n}_i^{\boldsymbol{Y}} \otimes \boldsymbol{n}_i^{\boldsymbol{Y}}, \quad \mathbb{A}_{d_{ijkl}} = \left(\delta_{ik} - D_{r_{ik}}\right)\left(\delta_{jl} - D_{r_{jl}}\right). \tag{19}$$

In the latter equation, Y_i and $\boldsymbol{n}_i$ denote the eigenvalues and eigenvectors of $\boldsymbol{Y}$, respectively. Additionally, $\langle \bullet \rangle$ defines the Macaulay brackets and the fourth order tensor $\mathbb{A}_d$ equips the model with greater flexibility, whereby the definition in Equation (19) is given with respect to the Cartesian basis system. Similar to the plastic regime, the evolution equations are obtained by following the principle of maximum dissipation

$$\dot{\boldsymbol{D}}_r = \dot{\gamma}_d \frac{\partial \Phi_d}{\partial \boldsymbol{Y}} = \dot{\gamma}_d\, \boldsymbol{Q}_+ \frac{\partial \Phi_d}{\partial \boldsymbol{Y}_+}\, \boldsymbol{Q}_+, \quad \dot{\kappa}_d = \dot{\gamma}_d \frac{\partial \Phi_d}{\partial R_d} = \dot{\gamma}_d \tag{20}$$

with the definition of the mapping tensor $\boldsymbol{Q}_+ = \sum_{i=1}^{3} \langle Y_i \rangle_H\, \boldsymbol{n}_i^{\boldsymbol{Y}} \otimes \boldsymbol{n}_i^{\boldsymbol{Y}}$, where $\langle \bullet \rangle_H$ is the Heaviside step function. The damage set of constitutive equations is closed by individual KKT conditions with the damage multiplier $\dot{\gamma}_d$.

2.3 Specific choices of energy terms

So far, the derivation of the model was kept quite general, in order not to restrict the model to a particular choice of energy terms. However, to study the model in a more detailed manner, the following energies are chosen

- Elastic energy: It is assumed that anisotropic damage results from isochoric deformations, while isotropic damage is associated with volumetric deformations (cf. e.g. [15]). In case of logarithmic strains, the energy can be easily decomposed into volumetric and isochoric deformations (cf. e.g. [16])

$$\psi_e = \mu_e \operatorname{tr}\Big(\operatorname{dev}\left(\bar{\boldsymbol{\eta}}_e\right)^2 (\boldsymbol{I} - \boldsymbol{D})\Big) + f_d \frac{K_e}{2} \operatorname{tr}\left(\bar{\boldsymbol{\eta}}_e\right)^2 \tag{21}$$

- Plastic energy: Chosen in line with the previous one but extended by an exponential hardening term

$$\psi_p = \mu_p \operatorname{tr}\Big(\operatorname{dev}\left(\boldsymbol{\eta}_p\right)^2 (\boldsymbol{I} - \boldsymbol{D})\Big) + f_d \frac{K_p}{2} \operatorname{tr}\left(\boldsymbol{\eta}_p\right)^2 + f_d\, r_p \left(\kappa_p + \frac{\exp\left(-s_p\, \kappa_p\right) - 1}{s_p}\right) \tag{22}$$

- Damage energy: Includes exponential and linear hardening, and moreover, a limit function for the eigenvalues D_i of $\boldsymbol{D}$ is involved

$$\psi_d = r_d \left(\kappa_d + \frac{\exp\left(-s_d\, \kappa_d\right) - 1}{s_d}\right) + \frac{H_d}{2}\, \kappa_d^2 + K_h \sum_{i=1}^{3} \left(-2\sqrt{1 - D_i} - D_i + 2\right) \tag{23}$$

- Micromorphic energy: Ensures a strong coupling of the 'local' variables with their 'nonlocal' counterparts, and further, introduces an internal length scale by taking the Lagrangian gradient of $\bar{\mathbf{d}}$ into account (cf. e.g. [14])

$$\psi_{\bar{d}} = \frac{H}{2} \sum_{i=1}^{3} \left(d_i - \bar{d}_i\right)^2 + \frac{A}{2} \sum_{i=1}^{3} \operatorname{Grad}\left(\bar{d}_i\right) \cdot \operatorname{Grad}\left(\bar{d}_i\right) \tag{24}$$

In the above, μ_e and K_e are the elastic shear and bulk modulus, μ_p and K_p can be interpreted analogously, while r_p, s_p, r_d, and s_d describe exponential hardening of plasticity and damage. Additionally, linear damage hardening is described by H_d and the eigenvalue limitation by K_h, while H is a penalty factor and A characterizes the internal length scale. The degradation function is given by $f_d = 1 - \frac{\operatorname{tr}(\boldsymbol{D})}{3}$.

2.4 Weak forms

The weak forms which need to be solved on a global level read as follows

$$g_u(\boldsymbol{u}, \bar{\mathbf{d}}, \delta\boldsymbol{u}) \coloneqq \int_{B_0} \boldsymbol{S} : \delta\boldsymbol{E}\, \mathrm{d}V - \int_{B_0} \boldsymbol{f}_0 \cdot \delta\boldsymbol{u}\, \mathrm{d}V - \int_{\partial_t B_0} \boldsymbol{t}_0 \cdot \delta\boldsymbol{u}\, \mathrm{d}A = 0 \tag{25}$$

$$g_{\bar{d}}(\boldsymbol{u}, \bar{\mathbf{d}}, \delta\bar{\mathbf{d}}) \coloneqq \int_{B_0} \boldsymbol{\xi}_{0_i} \cdot \delta\bar{\mathbf{d}}\, \mathrm{d}V + \int_{B_0} \boldsymbol{\Xi}_{0_i} : \operatorname{Grad}\left(\delta\bar{\mathbf{d}}\right)\, \mathrm{d}V = 0 \tag{26}$$

with the test functions $\delta\boldsymbol{u}$ and $\delta\bar{\mathbf{d}}$, the second Piola-Kirchhoff stress tensor $\boldsymbol{S}$, the virtual Green-Lagrange strain $\delta\boldsymbol{E} \coloneqq \operatorname{sym}\left(\boldsymbol{F}^T \operatorname{Grad}(\delta\boldsymbol{u})\right)$, the referential body force vector $\boldsymbol{f}_0$, and the referential traction vector $\boldsymbol{t}_0$. Both weak forms are nonlinear functions of their arguments, and thus, need to be solved using Newton-Raphson's method.

3 TRANSFORMATION OF ALGORITHMIC TANGENT OPERATORS

To be applicable in standard finite element formulations, the weak form of linear momentum (25) is stated in terms of Lagrangian quantities. In contrast, the entire constitutive framework is expressed in terms of logarithmic strain measures, and thus, the constitutively dependent variables as well as the material tangent operators need to be transformed to the Lagrangian space. Employing both that $\boldsymbol{\varepsilon}$ solely depends on $\boldsymbol{C} \coloneqq \boldsymbol{U}^2$ and the fact that the stress power in logarithmic and Lagrangian space has to be equal, the transformation of the second Piola-Kirchhoff stress is found

$$\dot{\boldsymbol{\varepsilon}} = \underbrace{2\frac{\partial\boldsymbol{\varepsilon}}{\partial\boldsymbol{C}}}_{=:\mathbb{Q}} : \frac{1}{2}\dot{\boldsymbol{C}}, \quad \boldsymbol{T} : \dot{\boldsymbol{\varepsilon}} \overset{!}{=} \boldsymbol{S} : \frac{1}{2}\dot{\boldsymbol{C}} \quad \rightarrow \quad \boldsymbol{S} = \boldsymbol{T} : \mathbb{Q}. \tag{27}$$

Since the evolution equations introduced in Section 2.2 are discretized in time within a time interval $t \in [t_n, t_{n+1}]$, the unknown variables which have to be solved on a local level are $\dot{\gamma}_{p_{n+1}}$, $\boldsymbol{\varepsilon}_{p_{n+1}}$, $\dot{\gamma}_{d_{n+1}}$, and $\boldsymbol{D}_{r_{n+1}}$. All of them being discretized using the backward Euler method. Algorithmically, these variables are implicit functions of $\boldsymbol{C}_{n+1}$ and $\bar{\mathbf{d}}_{n+1}$. Hence, in an algorithmic sense, one may write $\boldsymbol{S}_{n+1} = \bar{\boldsymbol{S}}_{n+1}\left(\boldsymbol{C}_{n+1}, \bar{\mathbf{d}}_{n+1}\right)$ as well as $\mathbf{d}_{n+1} = \breve{\mathbf{d}}_{n+1}\left(\boldsymbol{C}_{n+1}, \bar{\mathbf{d}}_{n+1}\right)$. In analogy, the logarithmic stress reads $\boldsymbol{T}_{n+1} = \bar{\boldsymbol{T}}_{n+1}\left(\boldsymbol{\varepsilon}_{n+1}, \bar{\mathbf{d}}_{n+1}\right)$. A straightforward incrementation of these latter equations leads to the following expressions

$$\Delta\boldsymbol{S} = 2\frac{\partial\boldsymbol{S}_{n+1}}{\partial\boldsymbol{C}_{n+1}} : \frac{1}{2}\Delta\boldsymbol{C} + \frac{\partial\boldsymbol{S}_{n+1}}{\partial\bar{\mathbf{d}}_{n+1}} \cdot \Delta\bar{\mathbf{d}}, \quad \Delta\mathbf{d} = 2\frac{\partial\mathbf{d}_{n+1}}{\partial\boldsymbol{C}_{n+1}} : \frac{1}{2}\Delta\boldsymbol{C} + \frac{\partial\mathbf{d}_{n+1}}{\partial\bar{\mathbf{d}}_{n+1}} \cdot \Delta\bar{\mathbf{d}} \tag{28}$$

with the global increments $\Delta\boldsymbol{C}$ and $\Delta\bar{\mathbf{d}}$. Following a similar procedure for $\boldsymbol{T}_{n+1}$ and $\mathbb{Q}_{n+1}$, the increments of $\boldsymbol{S}_{n+1}$ and $\mathbf{d}_{n+1}$, taking into account Equation (27), can also be written as

$$\begin{aligned}\Delta\boldsymbol{S} = \Delta\boldsymbol{T}_{n+1} : \mathbb{Q}_{n+1} + \boldsymbol{T}_{n+1} : \Delta\mathbb{Q}_{n+1} &= \left(\mathbb{Q}_{n+1} : \frac{\partial\boldsymbol{T}_{n+1}}{\partial\boldsymbol{\varepsilon}_{n+1}} : \mathbb{Q}_{n+1} + \boldsymbol{T}_{n+1} : \overset{6}{\mathbb{L}}_{n+1}\right) : \frac{1}{2}\Delta\boldsymbol{C} \\ &+ \mathbb{Q}_{n+1} : \frac{\partial\boldsymbol{T}_{n+1}}{\partial\bar{\mathbf{d}}_{n+1}} \cdot \Delta\bar{\mathbf{d}}\end{aligned} \tag{29}$$

$$\Delta\mathbf{d} = \frac{\partial\mathbf{d}_{n+1}}{\partial\boldsymbol{\varepsilon}_{n+1}} : \mathbb{Q}_{n+1} : \frac{1}{2}\Delta\boldsymbol{C} + \frac{\partial\mathbf{d}_{n+1}}{\partial\bar{\mathbf{d}}_{n+1}} \cdot \Delta\bar{\mathbf{d}} \tag{30}$$

with the sixth order tensor $\overset{6}{\mathbb{L}} \coloneqq 4\frac{\partial^2\boldsymbol{\varepsilon}}{\partial\boldsymbol{C}\partial\boldsymbol{C}}$. Both $\mathbb{Q}$ and $\overset{6}{\mathbb{L}}$ can be determined analytically (cf. [17]), but require both eigenvalues and eigenvectors, and thus, are numerically expensive to determine. However, if one considers that $\boldsymbol{C}$ has no complex eigenvalues, the calculation can be implemented numerically extremely efficient by means of algorithmic differentiation using the trigonometric solution of the eigenvalue problem. A technique based on this type of approach to compute the matrix logarithm as well as its derivatives is presented in [18] using *generating functions*,

which is not only very efficient but also quite accurate in terms of numerics. The material tangent operators in the logarithmic space are obtained using the algorithmic differentiation tool *AceGen*.

4 NUMERICAL EXAMPLE

In this numerical example, a tensile specimen is considered in a three-dimensional setting, whose boundary value problem is taken from the literature [19] and is depicted in Figure 1. Hexahedral finite elements with trilinear shape functions are used for discretization. The tensile specimen is uniaxially constrained, while the displacement in y direction is increased over time. Furthermore, due to symmetry, only one eighth of the entire geometry is simulated. Noteworthy, only Neumann boundary conditions are considered for the micromorphic boundary value problem, which are set to zero.
The material parameters for this example are taken from [1, 14]: $\mu_e = 55000$ [MPa], $K_e = 61666.\bar{6}$ [MPa], $\mu_p = 62.5$ [MPa], $K_p = 0$ [MPa], $r_p = 125$ [MPa], $s_p = 5$ [-], $\sigma_{y0} = 100$ [MPa], $H_d = 1$ [MPa], $r_d = 5$ [MPa], $s_d = 100$ [-], $K_h = 0.1$ [MPa], $Y_0 = 2.5$ [MPa] as well as $A = 75$ [MPa mm^2] and $H = 10^5$ [MPa]. It should be noted that an additional parameter used for a Taylor expansion of damage hardening is $a_d = 0.9999999$ [-] (cf. [1]).
The specimen is loaded in a monotonic way, where the displacements at the outer edges are steadily increased. A careful mesh convergence is performed using 580, 4113, 13660, and 18510 finite elements, which is shown in Figure 2. The finite element mesh of the finest discretization is shown in Figure 3. It is appealing to recognize convergence in both the onset of damage and the amount of dissipation. At the end of the simulation, the structural specimen can be considered 'fully broken', since the final value of the load is about two percent of the maximum value reached during the loading and a clear crack going through the specimen can be observed. Moreover, Figure 3 provides the contour plots of the main damage components as well as the accumulated plastic strain at the end of simulation using the finest mesh. A strong necking is clearly visible in the middle of the specimen. In this context, $D_{r_{yy}}$ can be interpreted as cracks in the plane perpendicular to the loading direction, which is why this plane is the most degraded. Slightly less degraded is the component $D_{r_{zz}}$, while the component $D_{r_{xx}}$ merely reaches a value of 0.8 [-]. In addition, the accumulated plastic strain κ_p can be understood as a measure of plasticity evolved, which is most pronounced in the region of necking.
Overall, it can be concluded that the developed material model is capable of providing plausible results even in a three-dimensional context.

5 CONCLUSION

Within this contribution, the model of [1], which couples elasto-plasticity to anisotropic damage for initially isotropic materials, was discussed in further detail. In addition, pathological mesh-dependency was cured by gradient-extended invariants of the second order damage tensor, resulting in three global unknowns in addition to the displacement field.
First of all, it was shown that the mapping for the damage tensor chosen in [1] indeed is invariant with respect to superimposed rotations of the intermediate configuration. Noteworthy, assuming an additive decomposition of the total strain does not harm the findings made in any way. As a consequence, it is not necessary to make any assumptions about, for instance, the plastic spin.

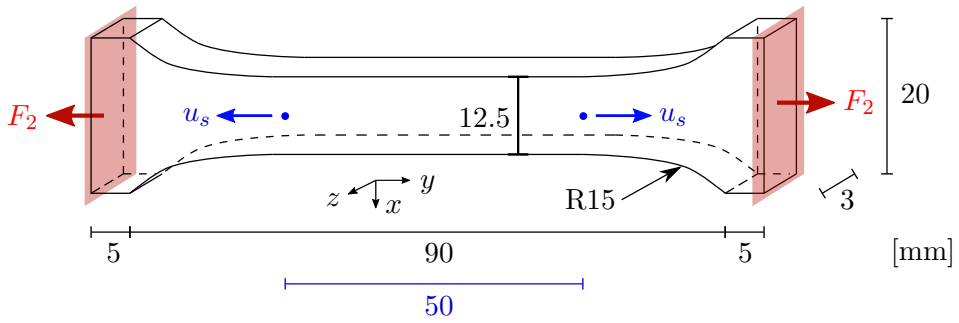

Figure 1: Geometry and boundary value problem. The specimen is loaded uniaxially, while the red edges remain perpendicular to the red forces. The displacements u_s (blue) are measured halfway between the center and the outer (red) edges of the specimen. The forces (red) are measured at the outer edges. Due to symmetry, only one eighth of the geometry is simulated.

Moreover, an alternative choice of the invariants used for gradient-extension was discussed here, which is based on the volumetric-deviatoric decoupling of the second order damage tensor.
For the numerical implementation, the weak form of linear momentum was expressed in terms of Lagrangian quantities, in order to be able to use the proposed model in standard finite element formulation. Therefore, the Lagrangian strains must be transformed to the logarithmic space and both the constitutively dependent variables as well as their algorithmic consistent tangent operators vice versa. In order to decrease the numerical effort required, it might be suitable to work with a combination of *generating functions* and algorithmic differentiation.
Lastly, the material model was examined in a three-dimensional numerical example to assess the ability of the proposed gradient-extension to cure mesh-dependency. Since coupled damage-plasticity simulations generally are very expensive in terms of numerical computation time, future works should focus on how to decrease the numerical effort, for instance, using adaptive mesh refinement or reduced integration (see e.g. [20]).

Acknowledgements. The authors gratefully acknowledge financial support by the German Science Foundation (DFG) (RE 1057/46-1, Project number 404502442). In addition, S. Reese and T. Brepols acknowledge the funding of the project RE 1057/51-1 (DFG, Project number 453715964).

REFERENCES

[1] H. Holthusen, T. Brepols, S. Reese, and J.-W. Simon. A two-surface gradient-extended anisotropic damage model using a second order damage tensor coupled to additive plasticity in the logarithmic strain space. *Journal of the Mechanics and Physics of Solids*, (2022) **163**:104833.

[2] H. Holthusen, T. Brepols, S. Reese, and J.-W. Simon. A novel gradient-extended anisotropic two-surface damage-plasticity model for finite deformations. *In: COMPLAS 2021*, (2022) 1-12.

[3] S. Forest. Micromorphic approach for gradient elasticity, viscoplasticity, and damage. *Jour-*

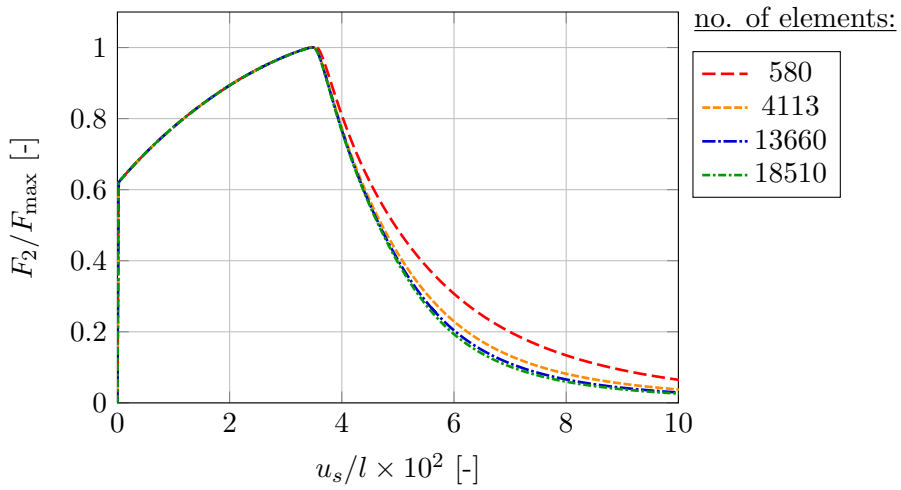

Figure 2: Normalized force-displacement curves with maximum load $F_{\max} = 6.044$ [kN]. Note that this value corresponds to the value of the whole geometry and not to the eighth, if symmetry is exploited. The latter corresponds to a quarter of $F_{\max}$. The displacement is normalized to the total length of the specimen $l = 100$ [mm]. For 18510 finite elements, the final value is about 0.02 [-]. The displacement u_s is indicated in Figure 1.

nal of Engineering Mechanics, (2009) **135**(3):117–131.

[4] S. Murakami. Mechanical Modeling of Material Damage. *Journal of Applied Mechanics*, (1988) **55**(2):280–286.

[5] H. Badreddine, K. Saanouni, and T. D. Nguyen. Damage anisotropy and its effect on the plastic anisotropy evolution under finite strains. *International Journal of Solids and Structures*, (2015) **63**:11–31.

[6] H. Holthusen, T. Brepols, S. Reese, and J.-W. Simon. An anisotropic constitutive model for fiber-reinforced materials including gradient-extended damage and plasticity at finite strains. *Theoretical and Applied Fracture Mechanics*, (2020) **108**:102642.

[7] L. Poggenpohl, H. Holthusen, and J.-W. Simon. Failure zone homogenization for modeling damage- and debonding-induced softening in composites including gradient-extended damage at finite strains. *International Journal of Plasticity*, (2022) **154**:103277.

[8] S. Reese, T. Brepols, M. Fassin, L. Poggenpohl and S. Wulfinghoff. Using structural tensors for inelastic material modeling in the finite strain regime – a novel approach to anisotropic damage. *Journal of the Mechanics and Physics of Solids*, (2021) **146**:104174.

[9] S. Forest. Nonlinear regularization operators as derived from the micromorphic approach to gradient elasticity, viscoplasticity and damage. *Proceedings of the Royal Society A: Mathematical, Physical and Engineering Sciences*, (2016) **472**(2188):20150755.

[10] C. Miehe, N. Apel, and M. Lambrecht. Anisotropic additive plasticity in the logarithmic strain space: modular kinematic formulation and implementation based on incremental

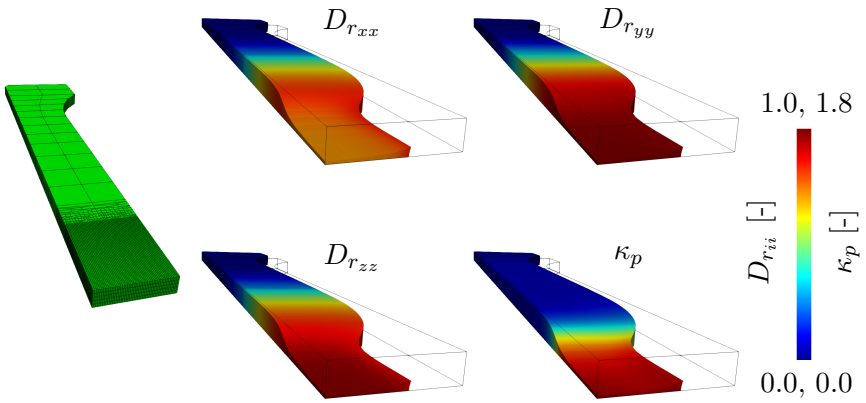

Figure 3: Left: Finite element mesh with 18510 elements, five layers are used in thickness direction. Middle: Contour plots of damage components $D_{r_{xx}}$, $D_{r_{yy}}$, $D_{r_{zz}}$, and accumulated plastic strain κ_p at the end of simulation ($u_s = 10$ [mm]). The maximum value of 1.0 [-] corresponds to the damage values, while 1.8 [-] is the maximum plastic strain value. Thin black lines illustrate the initial geometry.

minimization principles for standard materials. *Computer Methods in Applied Mechanics and Engineering*, (2002) **191**(47):5383 – 5425.

[11] J. Friedlein, J. Mergheim, and P. Steinmann. Observations on additive plasticity in the logarithmic strain space at excessive strains. *International Journal of Solids and Structures*, (2022) **239-240**:111416.

[12] M. Fassin, R. Eggersmann, S. Wulfinghoff, and S. Reese. Gradient-extended anisotropic brittle damage modeling using a second order damage tensor – theory, implementation and numerical examples. *International Journal of Solids and Structures*, (2019) **167**:93 – 126.

[13] K. Langenfeld and J. Mosler. A micromorphic approach for gradient-enhanced anisotropic ductile damage. *Computer Methods in Applied Mechanics and Engineering*, (2020) **360**:112717.

[14] T. Brepols, S. Wulfinghoff, and S. Reese. A gradient-extended two-surface damage-plasticity model for large deformations. *International Journal of Plasticity*, (2020) **129**:102635.

[15] R. Desmorat. Anisotropic damage modeling of concrete materials. *International Journal of Damage Mechanics*, (2016) **25**(6):818–852.

[16] J. C. Criscione, J. D. Humphrey, A. S. Douglas and W. C. Hunter. An invariant basis for natural strain which yields orthogonal stress response terms in isotropic hyperelasticity. *Journal of the Mechanics and Physics of Solids*, (2000) **48**(12):2445-2465.

[17] C. Miehe and M. Lambrecht. Algorithms for computation of stresses and elasticity moduli in terms of seth–hill's family of generalized strain tensors. *Communications in Numerical Methods in Engineering*, (2001) **17**(5):337–353.

[18] B. Hudobovnik and J. Korelc. Closed-form representation of matrix functions in the formulation of nonlinear material models. *Finite Elements in Analysis and Design*, (2016) **111**:19-32.

[19] S. Felder, N. Kopic-Osmanovic, H. Holthusen, T. Brepols, and S. Reese. Thermomechanically coupled gradient-extended damage-plasticity modeling of metallic materials at finite strains. *International Journal of Plasticity*, (2022) **148**:103142.

[20] O. Barfusz, T. van der Velden, T. Brepols, H. Holthusen, and S. Reese. A reduced integration-based solid-shell finite element formulation for gradient-extended damage. *Computer Methods in Applied Mechanics and Engineering*, (2021) **382**:113884.